KEEP THIS COPY FOR REPRODUCTION PURPOSES

ON PAGE

Form Approved
OMB No. 0704-0188



| 1. AGENCY USE ONLY (Leave blank) | 2. REPORT DATE | 3. REPORT TYPE AND DATES COVERED |
|---|---|---|
| | May 6, 1994 | |

**4. TITLE AND SUBTITLE**

Unsteady Flow Phenomena in Discrete Passage Diffusers for Centrifugal Compressors

**5. FUNDING NUMBERS**



**6. AUTHOR(S)**

V. Filipenco, J.M. Johnston, E.M. Greitzer

**7. PERFORMING ORGANIZATION NAME(S) AND ADDRESS(ES)**

Gas Turbine Laboratory
Massachusetts Institute of Technology
77 Massachusetts Ave.
Cambridge, MA 02139

**8. PERFORMING ORGANIZATION REPORT NUMBER**



**9. SPONSORING/MONITORING AGENCY NAME(S) AND ADDRESS(ES)**

U. S. Army Research Office
P. O. Box 12211
Research Triangle Park, NC 27709-2211

**11. SUPPLEMENTARY NOTES**

The view, opinions and/or findings contained in this report are those of the author(s) and should not be construed as an official Department of the Army position, policy, or decision, unless so designated by other documentation.

**12a. DISTRIBUTION/AVAILABILITY STATEMENT**

Approved for public release; distribution unlimited.

**12b. DISTRIBUTION CODE**



**13. ABSTRACT** *(Maximum 200 words)*

Research is described on the fluid dynamic behavior of high performance diffusers for centrifugal compressors, with particular application to small gas turbine engine applications. Using a unique swirl generator, experiments have been carried out to define the performance and stall onset behavior of a modern discrete passage diffuser as a function of inlet conditions. Two diffusers were examined, one with 30 passages and one with 38 passages. Inlet blockage and axial asymmetry were varied over Mach numbers up to unity and over a range of inlet swirl angles. Diffuser pressure recovery and operating range were calculated using traverse measurements made upstream of the diffuser. It was found that the performance of the diffuser under different inlet conditions could be expressed to a high degree of accuracy as a single curve of non-dimensional static pressure recovery coefficient, based on availability-averaged inlet stagnation pressure, and momentum-averaged inlet flow angle. Unsteady pressure measurements showed that the diffuser entered rotating stall at reduced flow rates. No long wavelength stall precursor was determined from the measurements.

**14. SUBJECT TERMS**

Centrifugal compressor diffusers, discrete passage diffuser performance, centrifugal compressor stall

**15. NUMBER OF PAGES**

37

**16. PRICE CODE**

| 17. SECURITY CLASSIFICATION OF REPORT | 18. SECURITY CLASSIFICATION OF THIS PAGE | 19. SECURITY CLASSIFICATION OF ABSTRACT | 20. LIMITATION OF ABSTRACT |
|---|---|---|---|
| UNCLASSIFIED | UNCLASSIFIED | UNCLASSIFIED | UL |

# UNSTEADY FLOW PHENOMENA IN DISCRETE PASSAGE DIFFUSERS FOR CENTRIFUGAL COMPRESSORS

FINAL REPORT

V. Filipenco, J.M. Johnston, E.M. Greitzer

May 1994

U.S. Army Research Office

Grant DAAL03-90-G-0138

Massachusetts Institute of Technology
Cambridge, MA 02139

# UNSTEADY FLOW PHENOMENA IN DISCRETE PASSAGE DIFFUSERS FOR CENTRIFUGAL COMPRESSORS

## – TABLE OF CONTENTS –

## LIST OF TABLES AND FIGURES

**Table**



**Figures**

**Figures (cont.)**

## ABSTRACT

Research is described on the fluid dynamic behavior of high performance diffusers for centrifugal compressors, with particular application to small gas turbine engine applications. Using a unique swirl generator, experiments have been carried out to define the performance and stall onset behavior of a modern discrete passage diffuser as a function of inlet conditions. Two diffusers were examined, one with 30 passages and one with 38 passages. Inlet blockage and axial asymmetry were varied over Mach numbers up to unity and over a range of inlet swirl angles. Diffuser pressure recovery and operating range were calculated using traverse measurements made upstream of the diffuser. It was found that the performance of the diffuser under different inlet conditions could be expressed to a high degree of accuracy as a single curve of non-dimensional static pressure recovery coefficient, based on availability-averaged inlet stagnation pressure, and momentum-averaged inlet flow angle. Unsteady pressure measurements showed that the diffuser entered rotating stall at reduced flow rates. No long wavelength stall precursor was determined from the measurements.


## INTRODUCTION AND PROBLEM STATEMENT

This document represents the final report on research sponsored by the Army Research Organization under Grant DAAL03-90-G-0138. The research addresses the fluid dynamic behavior of high performance discrete passage diffusers for centrifugal compressors, with particular application to small gas turbine engine applications. Experimental results are presented for a 30-passage and a 38-passage diffuser designed at an aircraft engine company.

### Background

The diffuser of a high performance centrifugal compressor often limits the machine's useful operating range due to the onset of aerodynamic instability, in the form of rotating stall or surge, at mass flow rates below design. Measurement of flow conditions at the inlet to the diffuser is difficult due to flow field sensitivity to instrumentation. The flow field of a centrifugal compressor is thus typically measured at the impeller inlet and at the diffuser exit to provide

designers with information about the impeller-diffuser combination. These measurements, however, do not isolate the individual component performances.

Defining the impeller and diffuser performance is desirable in design as well as when trying to optimize a tested machine by redesign. This performance split is often estimated based on some combination of static testing, calculated impeller and diffuser performances, and performance of previous designs, but little data appears to exist which shows clearly the effect of inlet conditions on diffusers. Testing a cascade passage diffuser in a manner in which the inlet conditions can be controlled is difficult due to the transonic inlet Mach numbers and high swirl angles characteristic of the impeller exit flow field. To address this problem, a test facility was constructed which enables determination of diffuser performance up to near sonic conditions (where the flow field is especially sensitive to instrumentation) and over a range of independently variable inlet flow conditions.

The results of the investigation have been reported in depth in Refs. [1] and [2]. For this reason the present report will not describe details of the design of the facility, nor give an extensive compilation of the results of the experiments. Rather, we will present an overview of the facility capability, and highlight the results which appear to be of most interest. The reader is referred to [1] or [2] for additional material which supplements this report.

## Research Objectives

One objective of the present study is to provide description of the causal links between centrifugal compressor diffuser behavior and inlet conditions. A second is to characterize the conditions that determine the limit of diffuser stable flow range. The variables of interest included inlet Mach number, inlet angle, inlet mass flow distribution, and instrumentation blockage. A third objective is to define the unsteady processes that are associated with the onset of instability (rotating stall or surge) of the diffuser flow field.

## EXPERIMENTAL APPARATUS

### Test Facility

The central elements of the test apparatus consists of a swirl generator which delivers an axisymmetric swirling transonic flow into the test section where the radial diffuser is installed. Reasons for the use of this method, as well as design goals, are given in Ref. [1]. The diffuser exit flow is dumped to a plenum and routed to a slave compressor, which can be activated to lower the diffuser back pressure. The overall scheme is depicted in Figure 1. The swirl generator, shown in Figure 2, consists of an inlet, a negative reaction impeller composed of 71 high solidity blades (Figure 3), a variable speed drive, and four slot rings for boundary layer control by mass injection or suction. Both suction and injection may be applied in an axisymmetric manner upstream and downstream of the impeller on either wall. The swirl generator operation envelope includes a maximum average exit Mach number of unity, and a range of (momentum) average inlet swirl angles up to 75 degrees.

In the description below, the axial direction is taken from the impeller hub, aft wall where $x = 0$, to the shroud forward wall where $x = b$. The positive tangential direction is clockwise aft looking forward, and zero degrees at top-dead-center. "Plane 1" is the swirl generator exit radius, which is the traverse probe radius. "Plane 2" is the diffuser exit radius upstream of the dump to the plenum. "Plane 1A" is the radius defined by the diffuser inlet circumferential static taps. "Plane 0" is the impeller exit. All other planes are explicitly called out.

### Radial Diffuser Geometry

There are four contiguous parts of the tested passage diffusers: the quasi-vaneless space, the throat, the diffuser, and the dump. Passage diffusers are defined along a centerline that is inclined at a large angle from a radial line. The quasi-vaneless space, which is designed to diffuse supersonic flow, is defined by the scalloped leading edges which span the passage width on either side of the passage (see Figure 4). The area converges to the throat, which fixes the maximum flow rate through the diffuser. The throat section is a cylinder with a length approximately equal to

its radius. Downstream of the throat, there is an expanding section which is a partial cone; the cone is cut by the two walls of diffuser which linearly diverge from the throat to the exit. The diffuser is thus a mix between a conical and a two dimensional diffuser, where most (over 85% for the 38-passage diffuser) of the area increase occurs in the tangential direction about the passage centerline. Table 1 lists the dimensions of the two diffusers used in the study.

**TABLE 1: DIFFUSER DIMENSIONS**

| Item | 30-passage Diffuser | 38-passage Diffuser |
|---|---|---|
| Inlet width | 0.354 inches | 0.354 inches |
| Inlet radius | 7.982 inches | 7.982 inches |
| Exit radius | 11.046 inches | 11.046 inches |
| Area ratio | 4.29 | 4.37 |
| Diffuser L/D | 8.75 | 9.44 |
| Diffuser throat diameter | 0.5057 inches | 0.4493 inches |
| Diffuser choking flow | 2.07 pps | 2.07 pps |

## Instrumentation

The swirl generator output was measured by a cylindrical, single hole probe, as shown in Figure 5, installed at a fixed tangential location, 0 degrees, at the diffuser inlet. The hole was moved axially to obtain the swirl angle and total pressure at fifteen points. At each axial station the probe was rotated to determine the pressure distribution on the cylinder. A second order polynomial was fit through the pressure distribution to determine the flow angle; fifth order and moving third order curve fits were used to obtain total pressure.

One passage, for each diffuser, had a line of seventeen static pressure taps down the centerline, with two in the throat region, as shown in Figure 6. There were also eight extra taps in the quasi vaneless space, and three additional taps at the diffuser exit. Twelve static taps, six on each wall, were placed circumferentially around the inlet of the diffuser. One static probe was inserted at the same radius as the traverse probe.

One high speed pressure transducer was placed in the plenum. Three high speed static

pressure transducers were installed in the vaneless space ring for the 30-passage diffuser testing. Five more were added for the 38-passage diffuser testing, although two of the original set were found to be inoperative.

The temperature was measured near the facility inlet screen and at one location in the plenum. A downstream venturi was used to measure mass flow.

## DEFINITION OF PARAMETERS

### Average Values

The inlet axial flow distribution could be controlled to achieve different levels of distortion velocity. The availability-averaged total pressure, as defined by Livesey and Hugh [3] and Filipenco [1]

$$\overline{Pt_{\psi 1}} = \exp\left[\frac{\int_0^b \ln\left(Pt_1(x)\right)\rho_1(x)V_{r1}(x)\,2\pi r_1 dx}{\int_0^b \rho_1(x)V_{r1}(x)\,2\pi r_1 dx}\right] \tag{1}$$

was used to define the diffuser pressure recovery coefficient,

$$Cpr_\psi = \frac{Ps_2 - Ps_1}{\overline{Pt_{\psi 1}} - Ps_1} \quad . \tag{2}$$

The diffuser average inlet swirl angle was found by taking the ratio of tangential and radial velocities mass weighted means, where

$$\overline{V_{\theta 1}} = \frac{\int_0^b \rho_1(x)V_{r1}(x)V_\theta(x)2\pi r_1 dx}{\int_0^b \rho_1(x)V_{r1}(x)\,2\pi r_1 dx} \tag{3}$$

and

$$\overline{V_{r1}} = \frac{\int_0^b \rho_1(x)V_{r1}(x)V_{r1}(x)2\pi r_1 dx}{\int_0^b \rho_1(x)V_{r1}(x)\,2\pi r_1 dx} \quad . \tag{4}$$

This averaging process implies a momentum weighted swirl angle,

$$\overline{\alpha_1} = \tan^{-1}\left(\frac{\overline{V_{\theta 1}}}{\overline{V_{r1}}}\right) \tag{5}$$

The diffuser inlet Mach number was calculated using $\overline{Pt_{\psi 1}}$

$$M_1 = \sqrt{\frac{2}{\gamma - 1}\left[\left(\frac{\overline{Pt_{\psi 1}}}{Ps_1}\right)^{\frac{\gamma-1}{\gamma}} - 1\right]} \tag{6}$$

**Profile Descriptors**

The inlet profiles of mass, momentum, energy, and swirl angle can be defined in terms of distortion parameters, which indicate the departure from uniformity, and skew parameters, which indicate the axial position about which the flow quality is equally divided. The inlet profile mass distortion parameter is

$$\sigma_m \equiv \frac{\int_0^b \left[(\rho V_r)_{max} - \rho(x)V_r(x)\right] 2\pi r_1 dx}{2\pi r_1 b(\rho V_r)_{max}} \; . \tag{7}$$

The inlet mass skew parameter is:

$$\xi_m \equiv \frac{x^*_m - b/2}{b/2} \tag{8}$$

where the location of the mass split line, $x^*_m$, satisfies

$$\int_0^{x^*_m} \rho(x)V_r(x)2\pi r_1 dx = \int_{x^*_m}^b \rho(x)V_r(x)2\pi r_1 dx \; . \tag{9}$$

Other parameters can be defined for momentum, kinetic energy and swirl angle, as given by Filipenco [1] or Johnston [2]. For example, the swirl angle distortion parameter used was the rms angle deviation from the momentum-averaged angle.

**Blockage Definitions**

Inlet blockage is a significant parameter for channel diffuser performance. For example, Sovran and Klomp [4] and Dolan and Runstadler [5] present data for two-dimensional and conical

diffusers which show decreasing diffuser static pressure coefficient with increasing boundary layer blockage at the diffuser inlet. In the present experiment, the boundary layer thickness is measured at the passage diffuser quasi-vaneless space inlet, not at the inlet of the channel part of the diffuser. In addition, for off-design high incidence cases, the boundary layer blockage associated with the flow around the scalloped leading edge may have a strong effect on overall diffuser performance.

As given by Dolan and Runstadler [5], the throat blockage is defined as

$$B = 1 - \left(\frac{\dot{m}_{actual}}{\dot{m}_{ideal}}\right)_{throat} \quad . \tag{10}$$

The throat blockage is not directly measured by this experiment. The actual mass flow is measured by the venturi. The ideal mass flow can be estimated as

$$\dot{m}_{ideal} = \sqrt{\frac{\gamma}{R}} \frac{Pt_1 A_1}{\sqrt{Tt_1}} \frac{M_1 \cos \overline{\alpha_1}}{\left(1 + \frac{\gamma - 1}{2} M_1^2\right)^{\frac{\gamma+1}{2(\gamma-1)}}} \quad . \tag{11}$$

The blockage at the quasi-vaneless space inlet is based on the mass flow from Eq. (11) using the availability-averaged total pressure (instead of the upstream reservoir total pressure used by Dolan and Runstadler). In addition, it is assumed that the flow is isentropic from the inlet to the throat, that the throat static pressure is equal to the lower of the two measured throat static pressures, and that the flow is essentially uni-directional at the throat.

## TEST PLAN

A series of constant corrected speed data sets (speed lines) were obtained for both diffusers. Boundary layer control was used to vary distortion parameter levels. Representative inlet swirl angle profiles for the no boundary layer control case and for two high skew cases are shown in Figure 7. The corresponding absolute Mach number profiles are also different from each other because the Mach number decreases as the swirl angle increases. The 30-passage diffuser testing had negative skew profiles, while the 38-passage diffuser testing included both positive and negative skews. A view of the range of inlet conditions is given in Figure 8 which shows the mass skew parameter as a function of mass distortion parameter for all data points, and

in Figure 9 (for the 38-passage diffuser) which shows the flow angle versus Mach number operating points for different suction and injection conditions. Each speed line consisted of a number of steady state operating points from choke to stall, including a near stall point. Three corrected speeds were examined: 2 KRPM, 4 KRPM, and 6 KRPM. Stall was detected by observing the output of one high speed pressure transducer, but it was also quite evident from decreased venturi mass flow and the plenum blow down. At the conclusion of the 38-passage diffuser test the traverse probe was removed and the 4 KRPM nominal and high distortion profiles speed lines were repeated. Unsteady data was measured without boundary layer control at several corrected speeds. Data was taken with and without the traverse probe being installed.

The flow delivered by the swirl generator was axisymmetric to a high degree. The inlet static pressure circumferential variation was typically less than 2% of the dynamic pressure, $\frac{1}{2}\rho V_1^2$, with the most variation being 4%. The two independent measurements of mass flow, the downstream venturi mass flow and the integrated inlet profile mass flow, agreed to within 5% for both diffuser tests; it may be noted that 0.5 degree error in the traverse angle would change the integrated inlet mass flow by 3.3% for a near stall swirl angle.

By applying suction aft of the impeller, it was possible to move the relative operating points of the diffuser and impeller separately. This technique was used to determine that it was the diffuser that initially encountered stall instability.

## RESULTS

### Steady-State Data

As discussed by Filipenco [1], a diffuser pressure recovery based on a dynamic pressure that used the availability total pressure provided a more general measure of diffuser performance than alternate dynamic pressure definitions (e.g. dynamic pressures based on the peak profile total pressure, area-averaged total pressure, or area-averaged velocity). At stall, the availability total pressure based diffuser recovery, $Cpr_\psi$ , decreased from 0.72 to 0.68 as the Mach number was increased from 0.15 to 0.80 under nominal conditions for the 30-passage diffuser, and to 0.67 at a

Mach number of 0.95.

Pressure recovery coefficients versus the inlet swirl angle for six speed lines, three without distortion and three with high distortion, are shown in Figure 10 The differences in speed (equivalent to Mach number) and profile distortion are collapsed by using the pressure coefficient based on availability total pressure; alternative definitions of recovery would lead to diffuser performance that varied versus speed and inlet distortion.

Pressure recovery coefficients for 20 near stall points with the 38-passage diffuser are shown as a function of inlet Mach number in Figure 11. (Note the expanded scales.) The diffuser pressure recovery coefficient decreases as the Mach number increases. No corresponding trend is observed for diffuser performance versus inlet mass distortion parameter, as shown in Figure 12. There is a weak trend of decreasing diffuser performance as the mass is skewed towards the impeller shroud, as given in Figure 13. In Figure 13, there are six pairs of points which comprise near stall points, at similar Mach number and inlet distortion parameter levels, which feature mass distributions that are reflected about the diffuser axial centerline, $x/b = 0.5$. Five of the six pairs indicate that when the mass distribution is skewed towards the impeller shroud, the diffuser does not perform as well. The one exception is where the near stall point for the negative skew case was not as close to stall, in terms of throttle closure, as the positive skew case. The extreme pairs, where suction and injection are applied, at 2 KRPM and 4 KRPM best illustrate the trend. The total data set of near stall points is shown in Figures 14 and 15 for both diffusers; the same general trends are exhibited for both.

The question of why diffuser performance is not sensitive to inlet distortion parameter is an issue of interest. The relation between the (calculated) blockage at the throat and the inlet mass distortion parameter is definitively not a strong one, particularly at off-design, as shown in Figure 16. We are currently examining this point; the idea is to "separate" the diffusion up to the throat from the diffusion downstream of the throat viewing the latter as similar to a channel diffuser.

Removing the traverse probe had a large effect on stall onset point. Near stall, axial motion of the traverse cylinder caused the diffuser to stall on repeated occasions. Typically, a near stall

operating point was set and the machine allowed to stabilize. The test sequence would begin and the traverse would start to move axially with the consequence that the diffuser would enter rotating stall immediately after the probe moved. To determine the effect of the circumferential distortion created by the traverse cylinder upon diffuser stall margin, the probe was removed and 4 KRPM speed lines with nominal inlet and both extreme skews were measured.

Without the traverse there is some uncertainty in determining the extent of inlet distortion for the skewed inlet distributions. Comparisons between the nominal inlet operating points are thus more meaningful but the mass flow operating range for both high skew cases increased by approximately 10% when the probe was not installed.

Removing the traverse probe increased the mass flow range by 15%, with the nominal inlet profile. Figure 17 shows the average diffuser inlet static pressure at plane 1A versus venturi mass flow for the 4 KRPM throttle for three cases: 30-passage diffuser with the traverse probe installed, 38-passage diffuser with the traverse probe installed, and 38-passage diffuser without the traverse probe installed.

No direct data is available for the 30-passage diffuser performance without the traverse probe. Only the throttle positions and the plane 1 static pressures are available, but these do indicate a similar mass flow range increase. At 4 KRPM, both diffusers stalled at a plane 1 pressure ratio of 0.985 with the traverse installed and both stalled at a plane 1 pressure ratio of 1.0 without the probe installed.

Indirect evidence is furnished from the 30-passage diffuser data taken with a bent traverse probe (i.e., larger blockage). The stalling flow for this configuration is estimated to be 30% higher than for the configuration without the probe (at a plane 1 pressure ratio of 0.95). The implication is that the diffuser may be more sensitive to steady circumferential distortion than to axial distortion.

Based on the measured swirl generator performance, the relationship of pressure recovery to venturi mass flow can be derived assuming that the flow in the vaneless space is isentropic. Utilizing this approach, the pressure recovery of the diffuser was estimated for the nominal inlet

operating points taken without the traverse probe installed, as shown in Figure 18. There is a 0.04 difference in pressure recovery, which is significant when viewed in terms of the length increase needed to obtain the same increase in peak recovery. A six degree conical diffuser with a peak pressure recovery coefficient of 0.71 would have to be 63% longer to reach the 0.75 pressure recovery level (Ref. [5] Figure 56, Mach number = 0.4, throat blockage = 0.03).

### Unsteady Flow Phenomena

Unsteady measurements were also taken to define the phenomena at stall onset. Intermittent small amplitude, long wavelength activity was observed before stall with no traverse probe installed. These waves moved in the opposite sense to the impeller rotation and the rotating stall waves. No coherent activity was evident prior to stall when the probe was installed, as seen in a typical time trace shown in Figure 19. The rotating stall instability was always first observed in the quadrant immediately in the direction of impeller rotation "downstream" of the probe. Prior to stall, the static pressure variations in this region were larger than in the other three quadrants. Removal of the probe eliminated the probe noise at the same throttle setting, as seen in Figure 20. With no probe, there was coherent activity on an intermittent basis prior to stall, as seen in Figure 21. Most of the energy was in the first and second mode, and appeared near the impeller rotation frequency. The inception process was short in duration, lasting about five rotor revolution times from first observation to essentially fully developed.

## SUMMARY AND CONCLUSIONS

A facility has been designed and constructed for examination of diffusers for high performance centrifugal compressors. The facility provides a transonic swirling flow at diffuser inlet, with control of inlet velocity profiles. Using this facility, the fluid dynamic behavior of two modern discrete passage diffusers has been assessed with primary focus on the effect of inlet conditions.

Definition of a pressure rise coefficient using an availability-averaged total pressure provided a generalized view of diffuser data for different Mach numbers and inlet distortion. The

mass-averaged total pressure was close to the availability-averaged total pressure, but area-averaged total pressure was quite different, i.e. $Cpr_{\psi} \cong Cpr_{mass} \neq Cpr_{area}$ .

There appears to be little relation between blockage, or mass distortion parameter, at the quasi-vaneless space inlet to the throat blockage. Efforts are now ongoing to define the relation between inlet quantities and the throat blockage; the latter is viewed as the main factor in the channel diffuser performance.

The effect of the probe on the stall onset implies that the stalls with the probe inserted are due to the probe wake. (The probe blockage is roughly 10% in terms of the probe cross-sectional area compared to the 38-passage diffuser throat area. Once the probe was removed the operational range increased and the stall mechanism changed.

No periodic activity was measured at the throttle setting where the diffuser stalled when the probe was inserted. As the throttle was closed, small amplitude, intermittent waves travelled in the opposite direction to impeller rotation were detected. Rotating stall inception occurred quickly, within five impeller revolutions of first evidence.

## PUBLICATIONS AND TECHNICAL REPORTS

Filipenco, V., "Experimental Investigation of Flow Distortion Effects on the Performance of Radial Discrete-Passage Diffusers," MIT Gas Turbine Laboratory Report No. 206, September 1991.

Johnston, J.M., "Stall Onset Observations of a Discrete Passage Diffuser," MIT Gas Turbine Laboratory Report No. 217, March 1993.

## PERSONNEL

E.M. Greitzer
V. Filipenco (Ph.D. Thesis)
J.M. Johnston (M.S. Thesis)
Y.C. Liang (M.S. Thesis expected 6/94)

## REFERENCES

1. Filipenco, V., "Experimental Investigation of Flow Distortion Effects on the Performance of Radial Discrete-Passage Diffusers," MIT Gas Turbine Laboratory Report No. 206, September 1991.

2. Johnston, J.M., "Stall Onset Observations of a Discrete Passage Diffuser," MIT Gas Turbine Laboratory Report No. 217, March 1993.

3. Livesey, J.L., Hugh, T., "'Suitable Mean Values' in One-Dimensional Gas Dynamics," *Journal Mechanical Engineering Science,* Vol. 8, No. 4, 1966.

4. Sovran, G., Klomp, E.D., "Experimentally Determined Optimum Geometries for Rectilinear Diffusers with Rectangular, Conical, or Annular Cross Section," in *Fluid Mechanics of Internal Flows*, G. Sovran, Ed., Elsevier, 1967.

5. Dolan, F.X., Runstadler, P.W., Jr., "Pressure Recovery Performance of Conical Diffusers at High Subsonic Mach Numbers," NASA Technical Report CR-2299, August 1973.

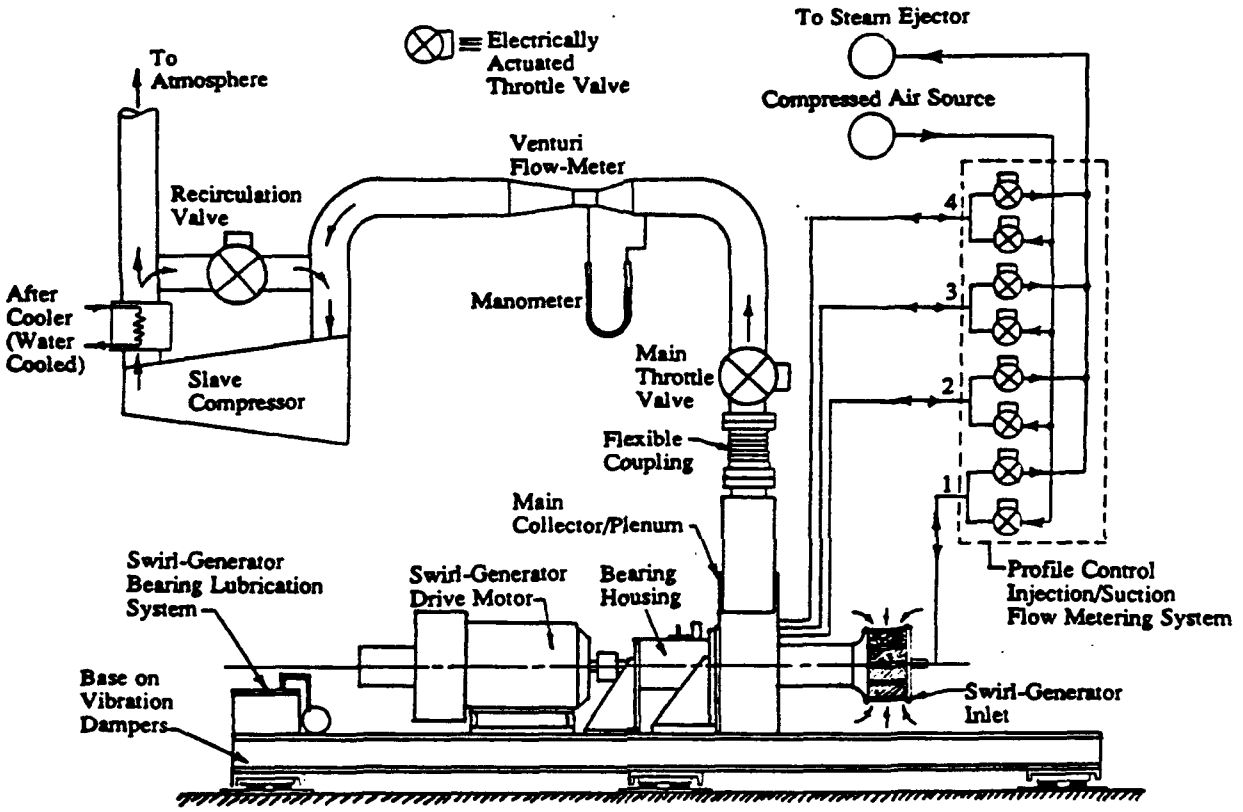


Figure 1: Piping schematic.

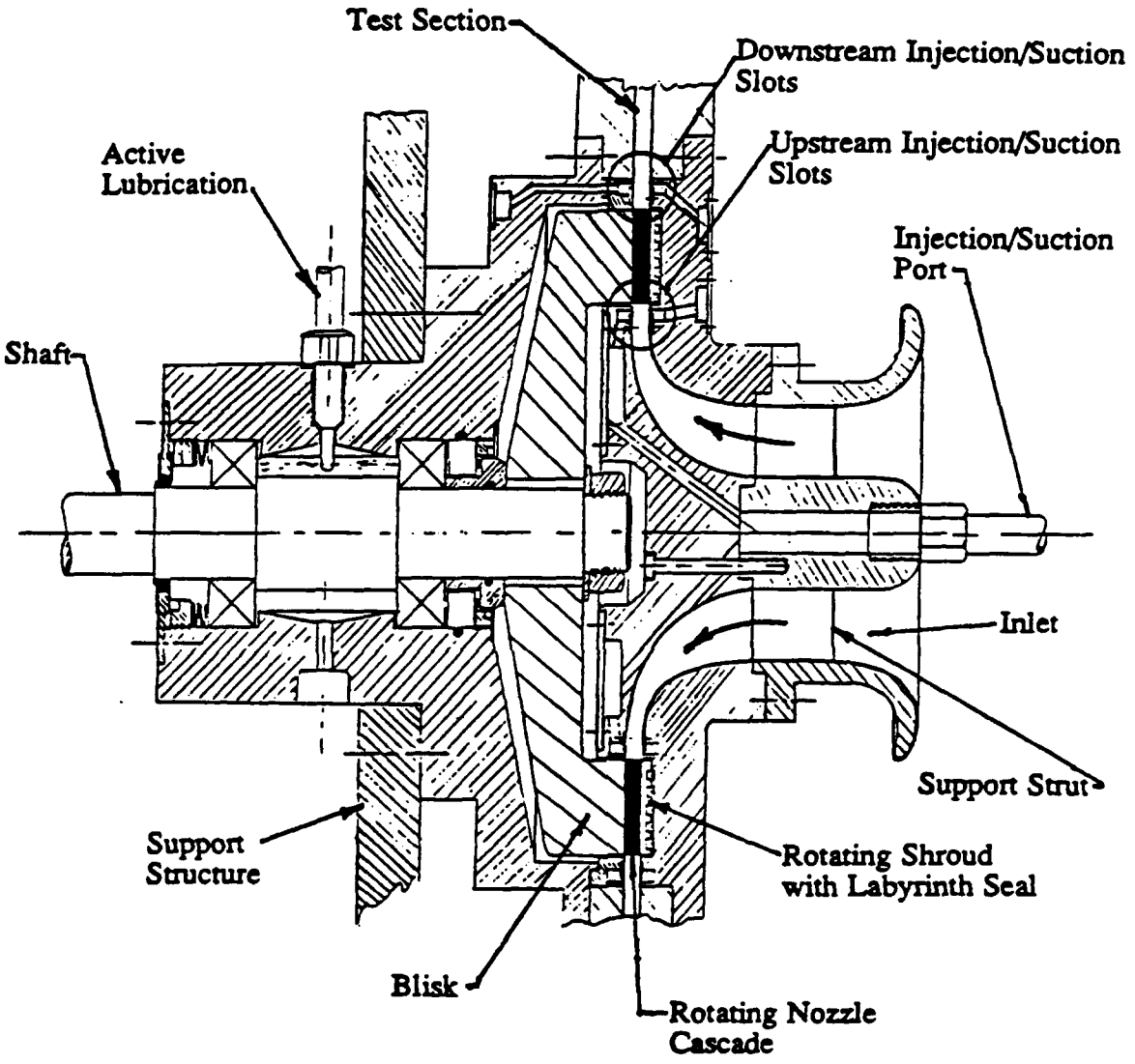


Figure 2: Swirl generator schematic.

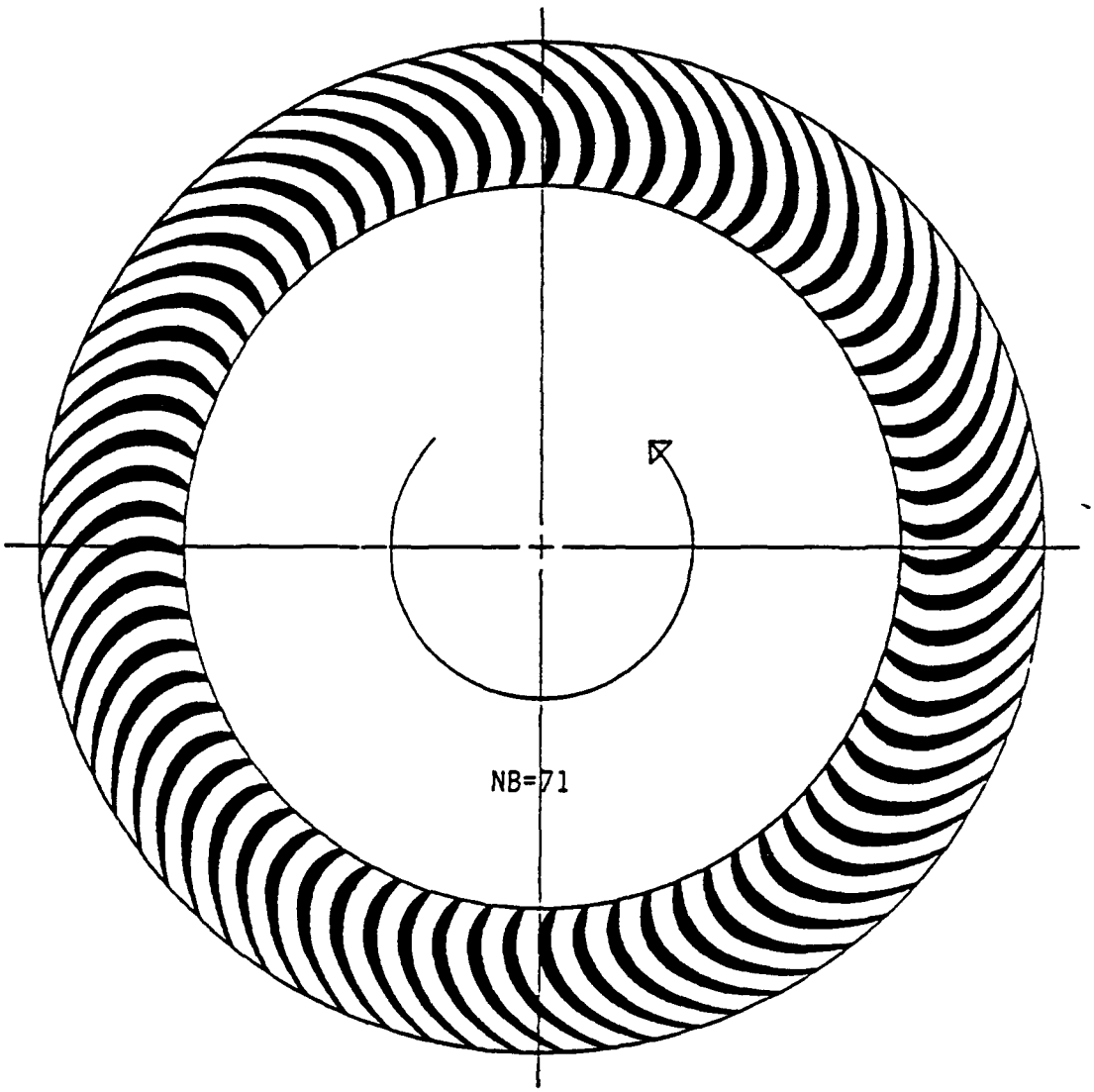


Figure 3: Impeller blade shapes.

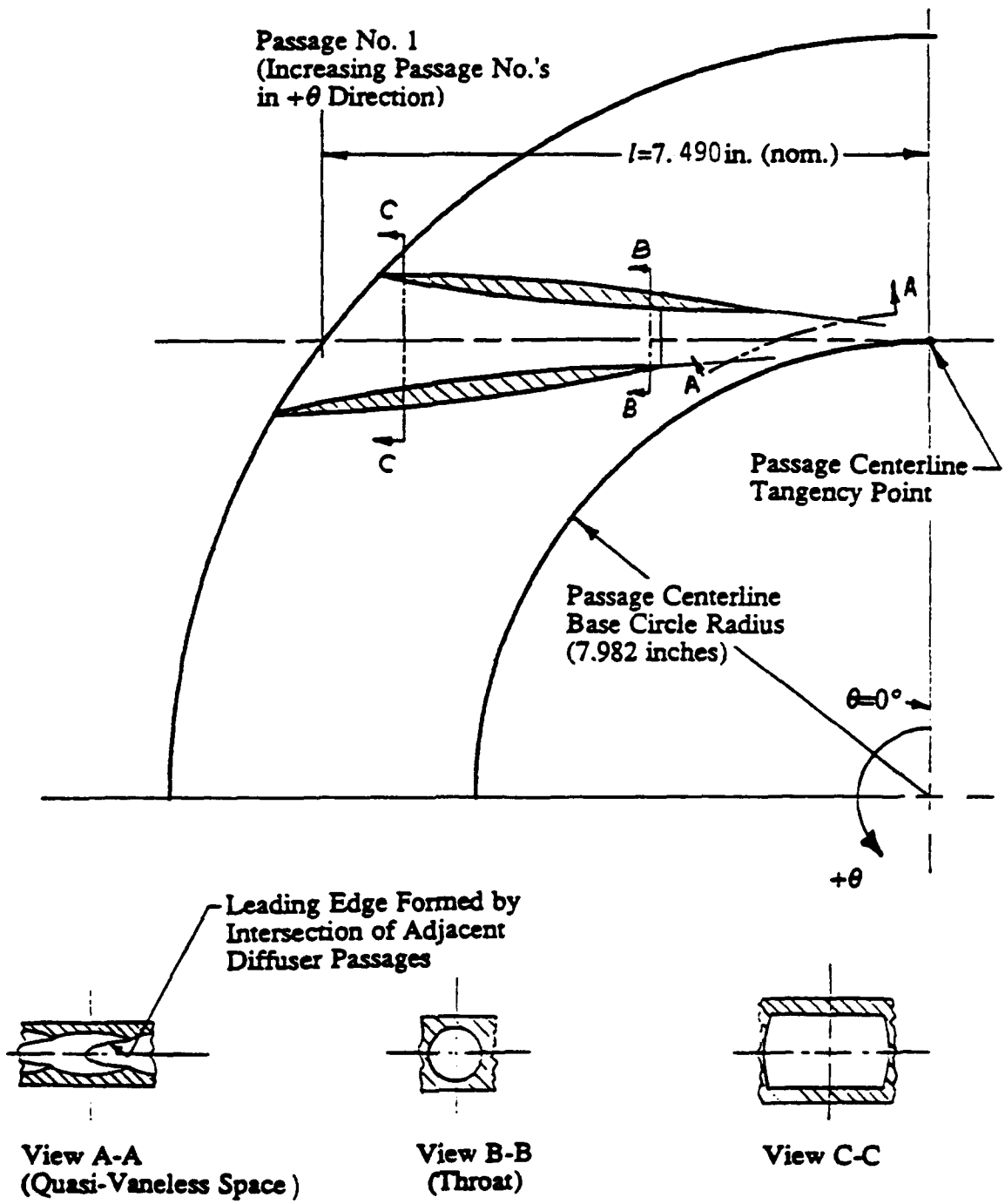


Figure 4: 38-passage diffuser geometry sketch.

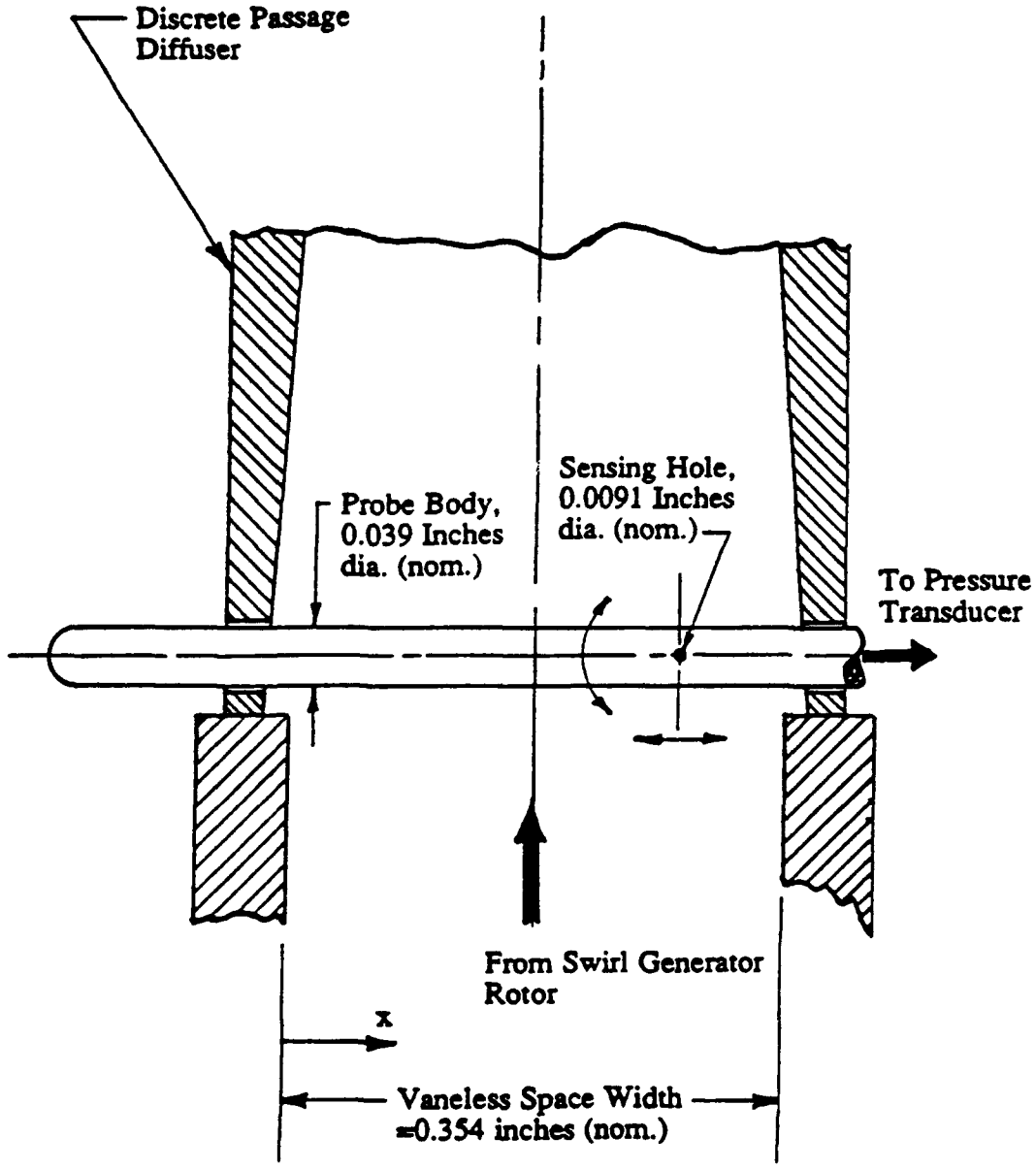


Figure 5: Traverse Probe.

| Tap No. | ξ | ζ | Tap No. | ξ | ζ |
|---|---|---|---|---|---|
| 1 | 0.803 | 0.057 | 16 | 3.393 | 0.0 |
| 2 | 1.023 | 0.083 | 17 | 3.850 | 0.0 |
| 3 | 1.314 | 0.102 | 18 | 4.300 | 0.0 |
| 4 | 1.544 | 0.134 | 19 | 4.750 | 0.0 |
| 5 | 1.250 | 0.0 | 20 | 5.210 | 0.0 |
| 6 | 1.540 | 0.0 | 21 | 5.660 | 0.0 |
| 7 | 1.837 | 0.0 | 22 | 6.200 | 0.0 |
| 8 | 1.637 | -0.071 | 23 | 6.693 | 0.0 |
| 9 | 2.131 | 0.0 | 24 | 7.186 | 0.0 |
| 10 | 1.927 | -0.084 | 25 | 7.186 | -0.275 |
| 11 | 2.424 | 0.0 | 26 | 7.186 | 0.275 |
| 12 | 2.218 | -0.092 | 27 | 7.490 | 0.0 |
| 13 | 2.846 | 0.0 | 28 | 7.728 | -0.230 |
| 14 | 2.519 | -0.113 | 29 | 7.952 | -0.460 |
| 15 | 3.268 | 0.0 | | | |

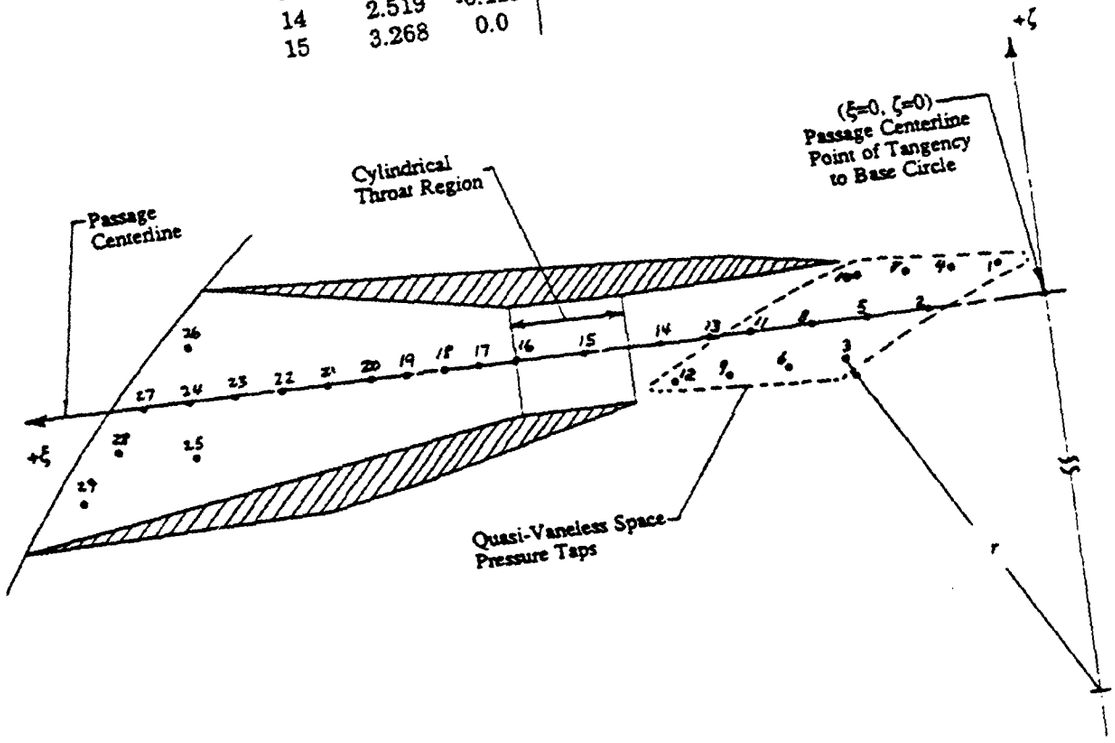


Figure 6: Passage #31 static tap location sketch.

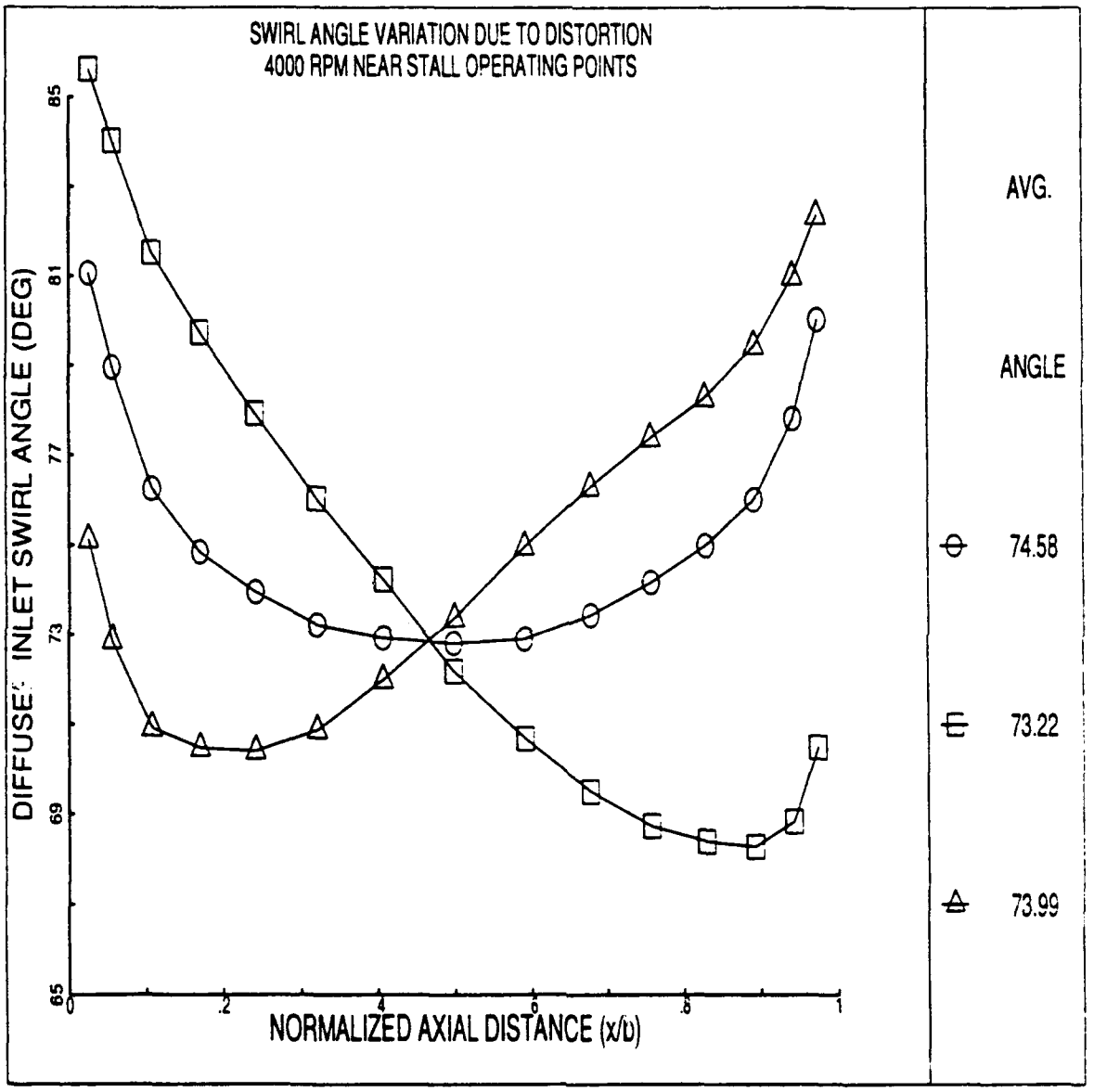


Figure 7: Variation in inlet angle versus axial position at 4 KRPM for three cases: ○ no boundary layer control, □ aft suction and forward injection, △ forward suction and aft suction.

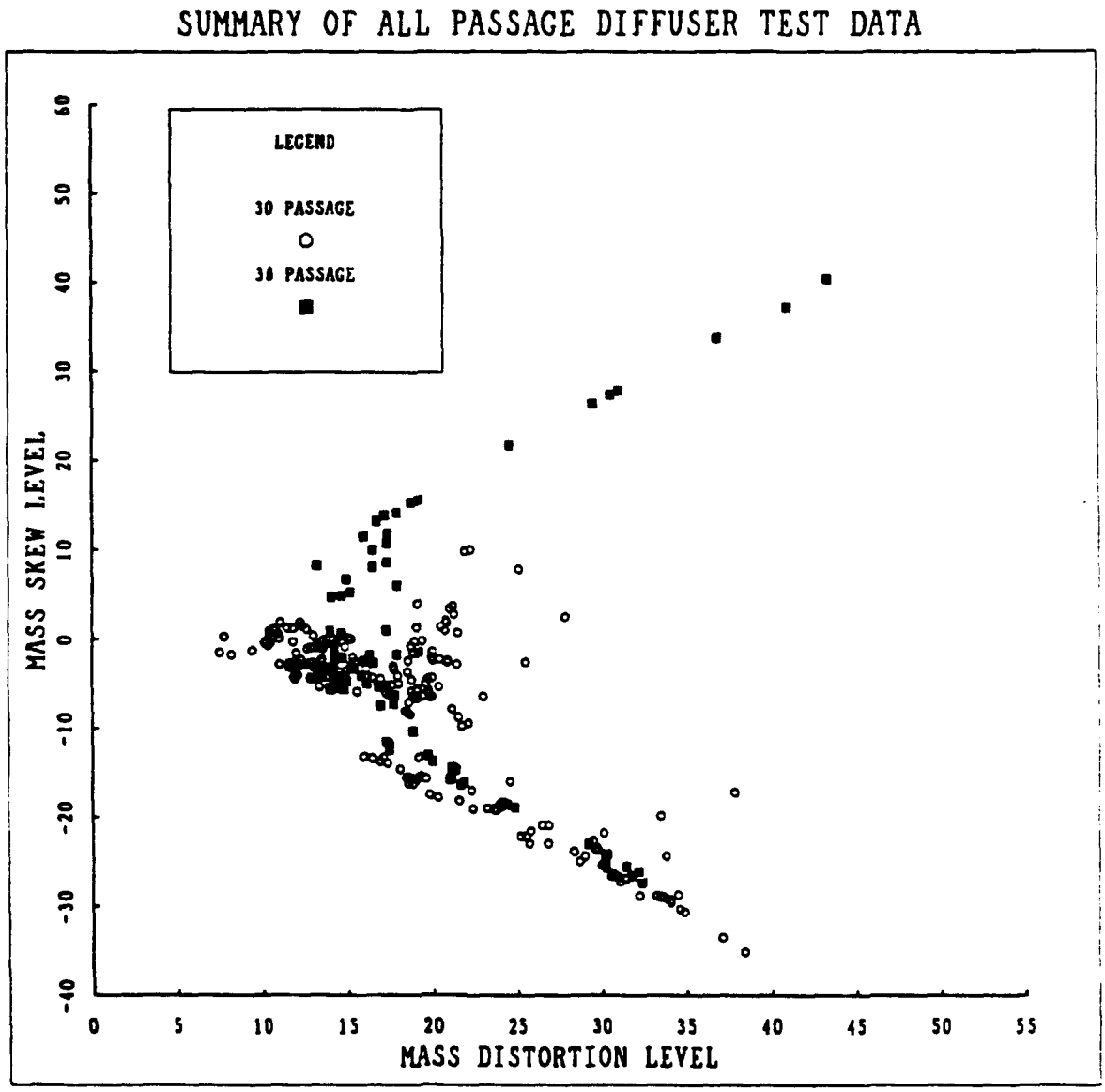


Figure 8: Summary plot of diffuser inlet conditions examined.

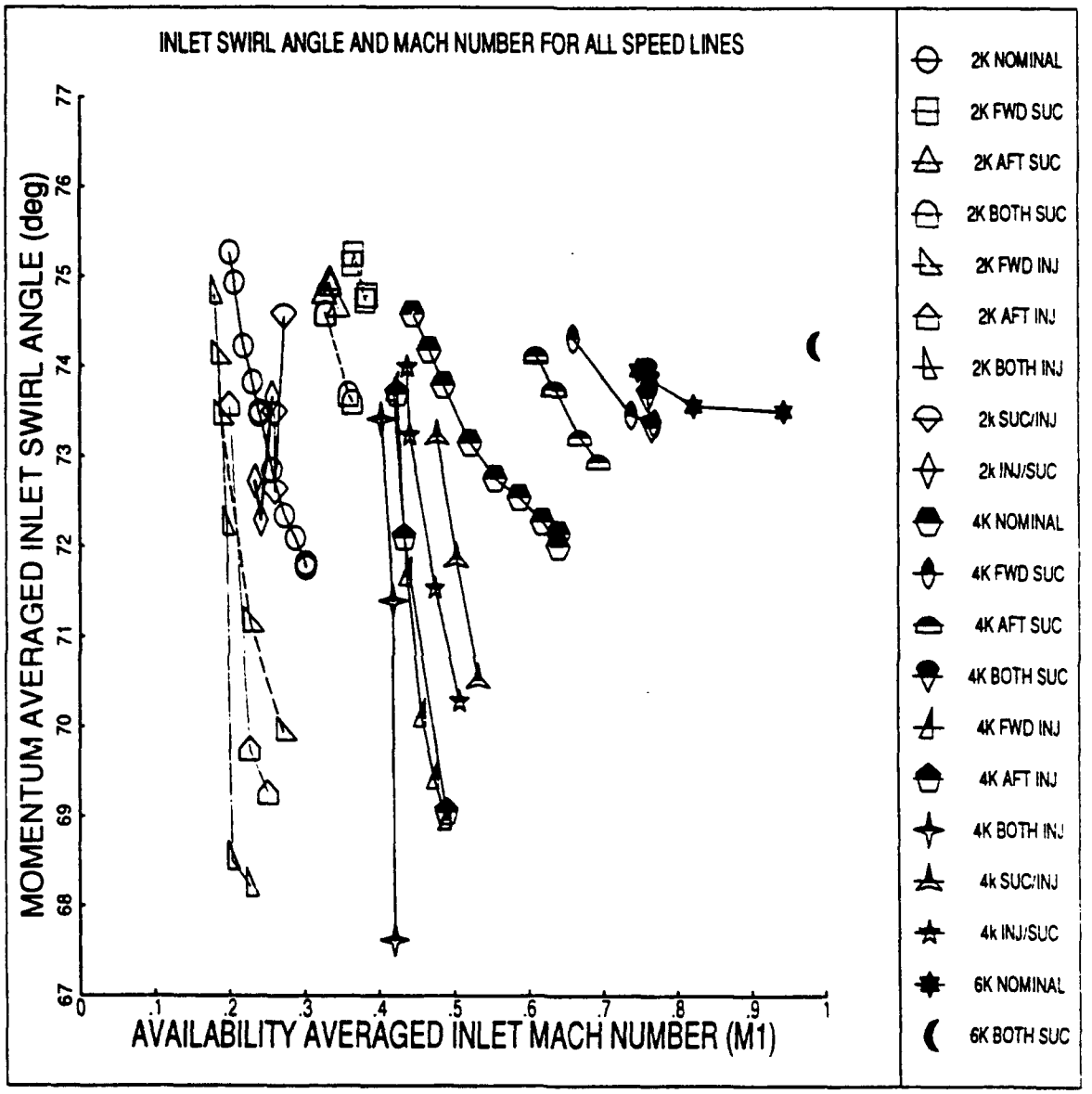


**Figure 9:** Flow conditions examined (38-passage diffuser): inlet swirl angle and inlet Mach number combinations. Legend indicates speed and inlet control, where K = 1 KRPM, inj = injection, suc = suction, FWD = shroud side (x/b = 1), and AFT = hub side (x/b = 0).

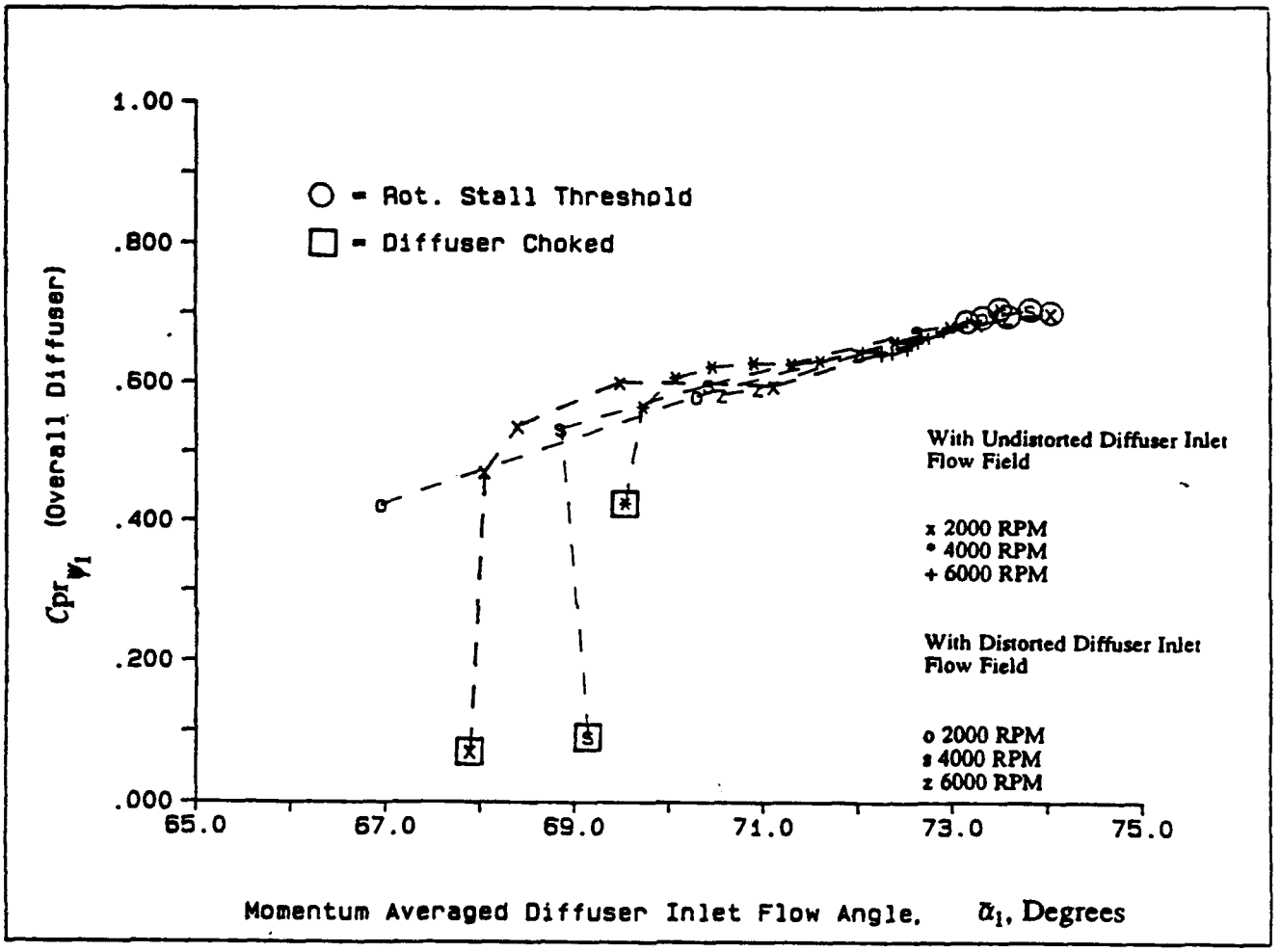


Figure 10: Diffuser overall, availability-averaged pressure recovery, $Cp_{\Psi}$, as a function of momentum-averaged inlet swirl angle (30-passage diffuser).

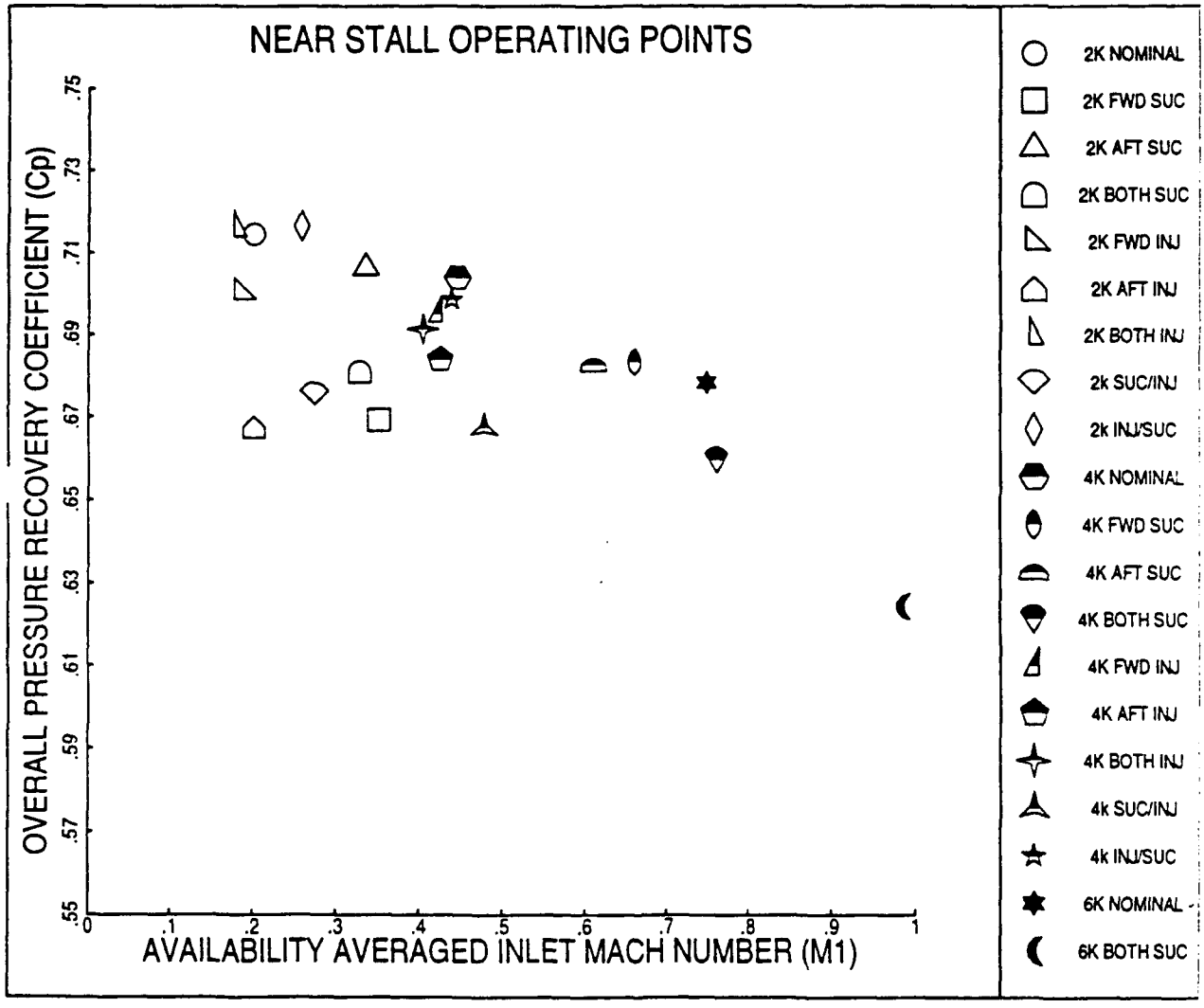


Figure 11: Near stall operating points, $Cp_{\psi}$ versus M1 for 38-passage diffuser. Legend indicates speed and inlet control, where K = 1 KRPM, inj = injection, suc = suction, FWD = shroud side (x/b = 1), and AFT = hub side (x/b = 0).

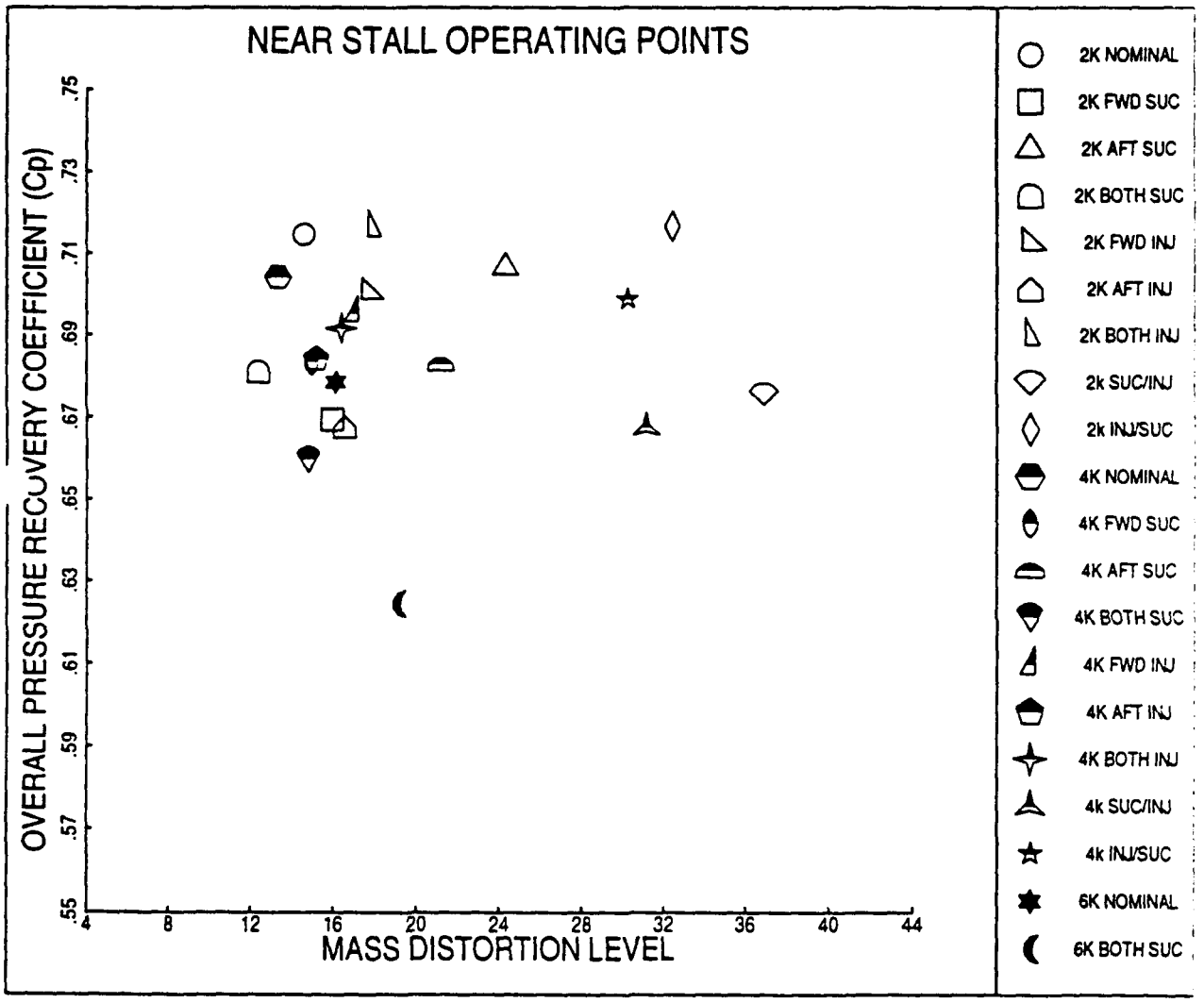


Figure 12: Pressure recovery coefficient at near stall points versus inlet mass flow distortion parameter. Legend indicates speed and inlet control, where K = 1 KRPM, inj = injection, suc = suction, FWD = shroud side (x/b = 1), and AFT = hub side (x/b = 0).

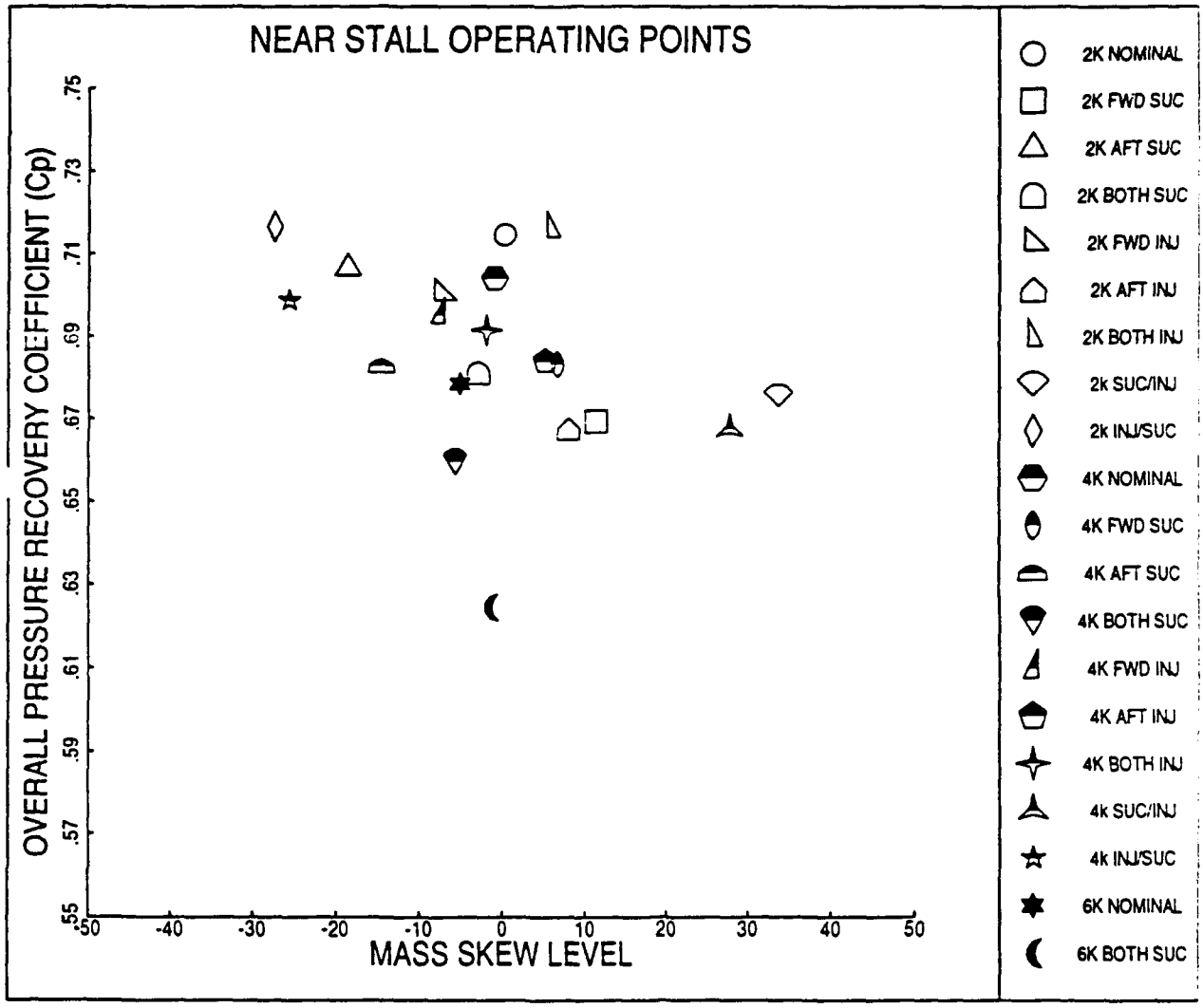


Figure 13: Pressure recovery coefficient at near stall points versus mass flow skew parameter. Legend indicates speed and inlet control, where K = 1 KRPM, inj = injection, suc = suction, FWD = shroud side (x/b = 1), and AFT = hub side (x/b = 0).

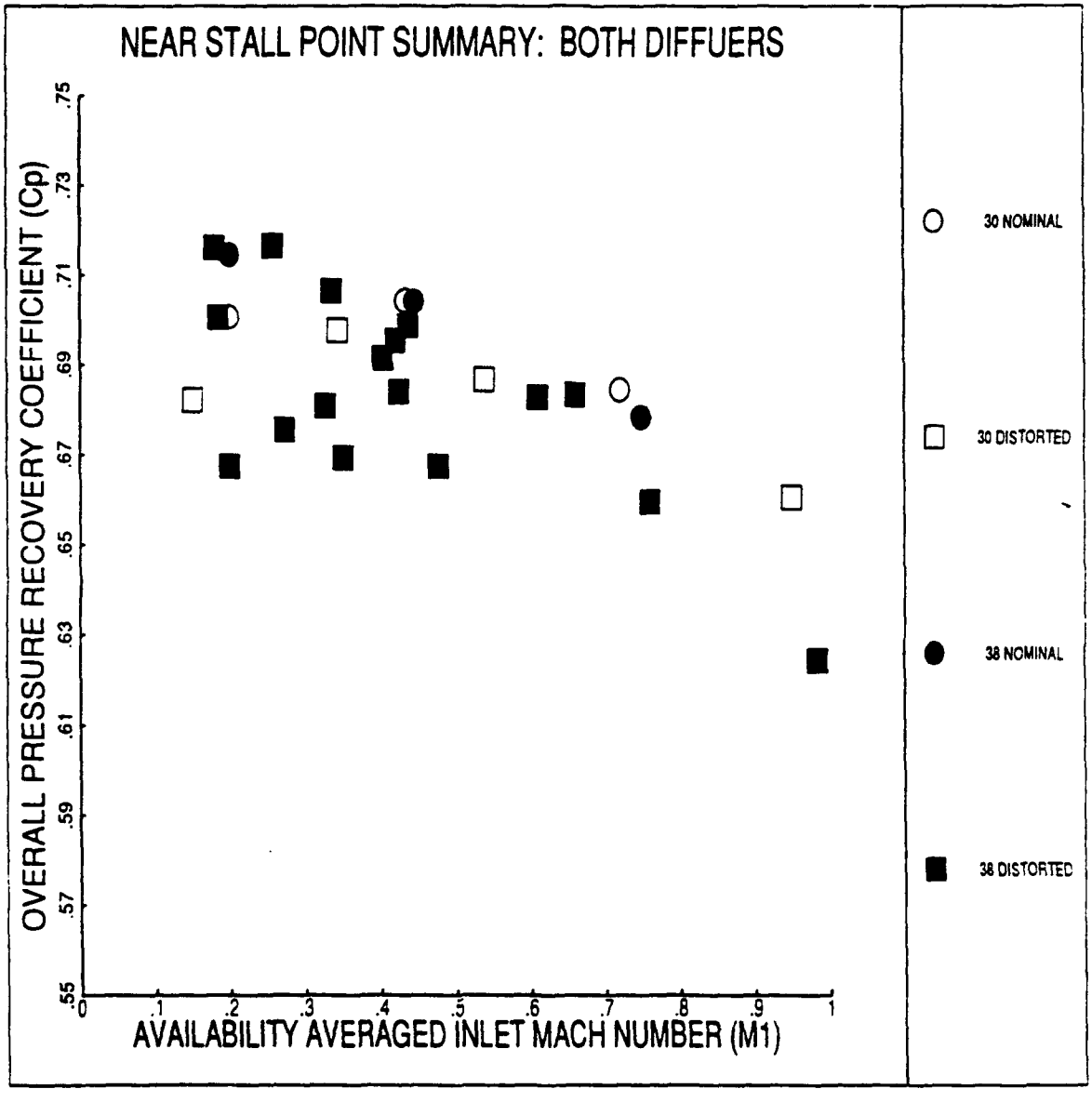


Figure 14: Comparison of diffuser near stall $Cp_\psi$ versus inlet Mach number for the 30-passage and the 38-passage diffusers. Nominal inlet conditions are indicated by circles, suction or injection is indicated by squares, and 38-passage data is indicated by shaded symbols.

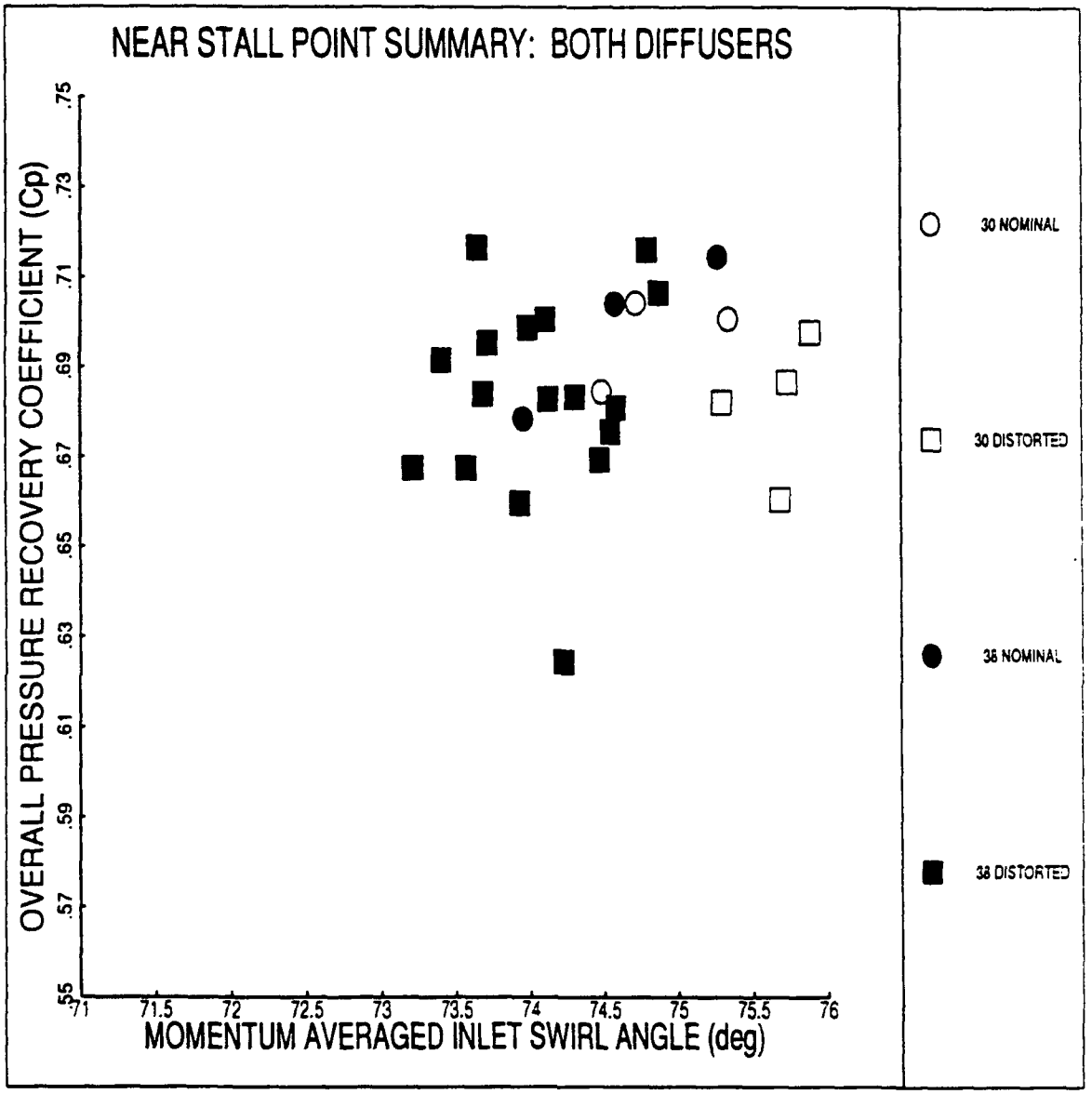


Figure 15: Comparison of near stall $Cp_\psi$ versus inlet swirl angle for the 30-passage and the 38-passage diffusers. Nominal inlet conditions are indicated by circles, suction or injection is indicated by squares, and 38-passage data is indicated by shaded symbols.

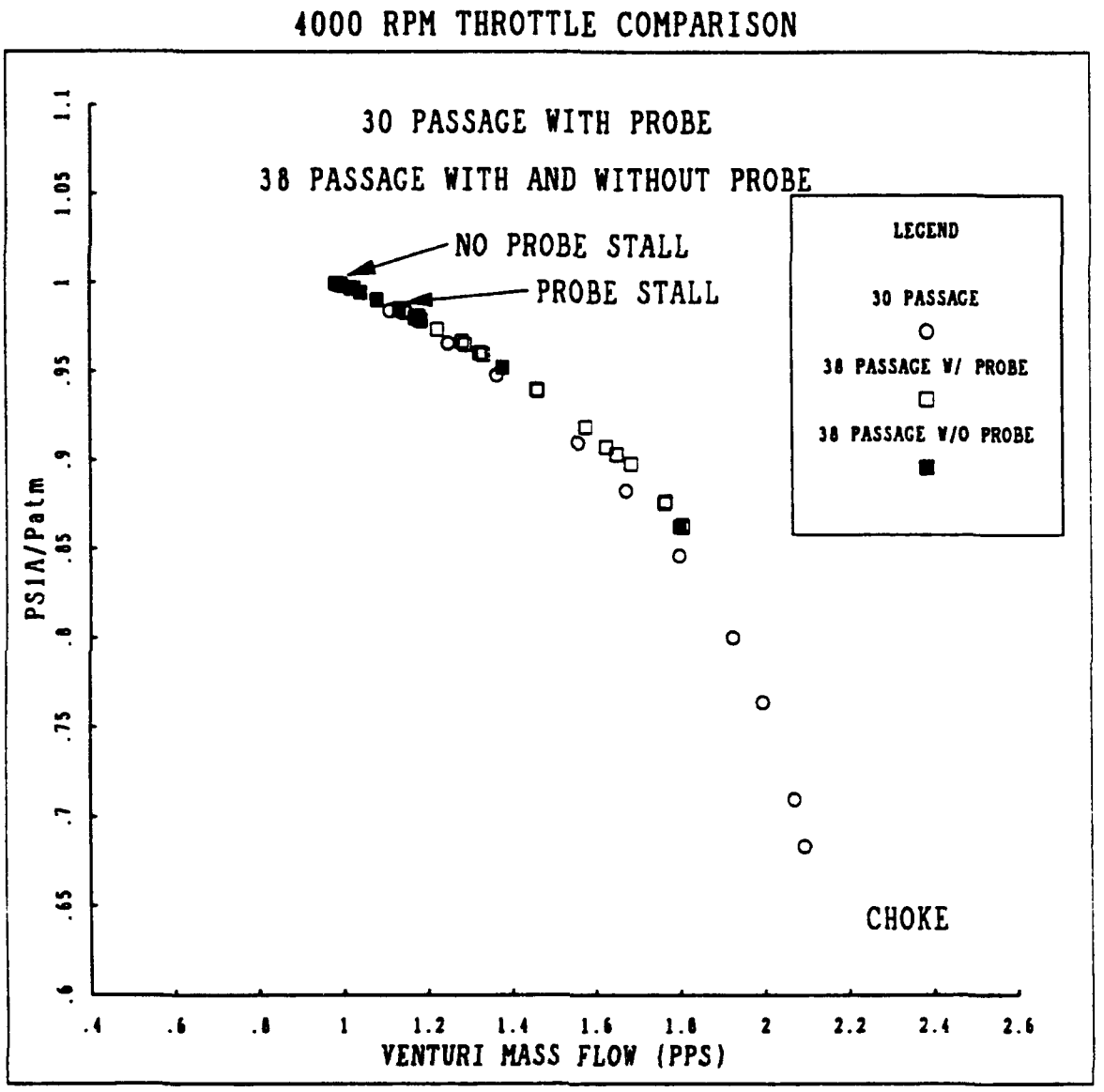


Figure 17: Diffuser mass flow range with and without traverse probe.

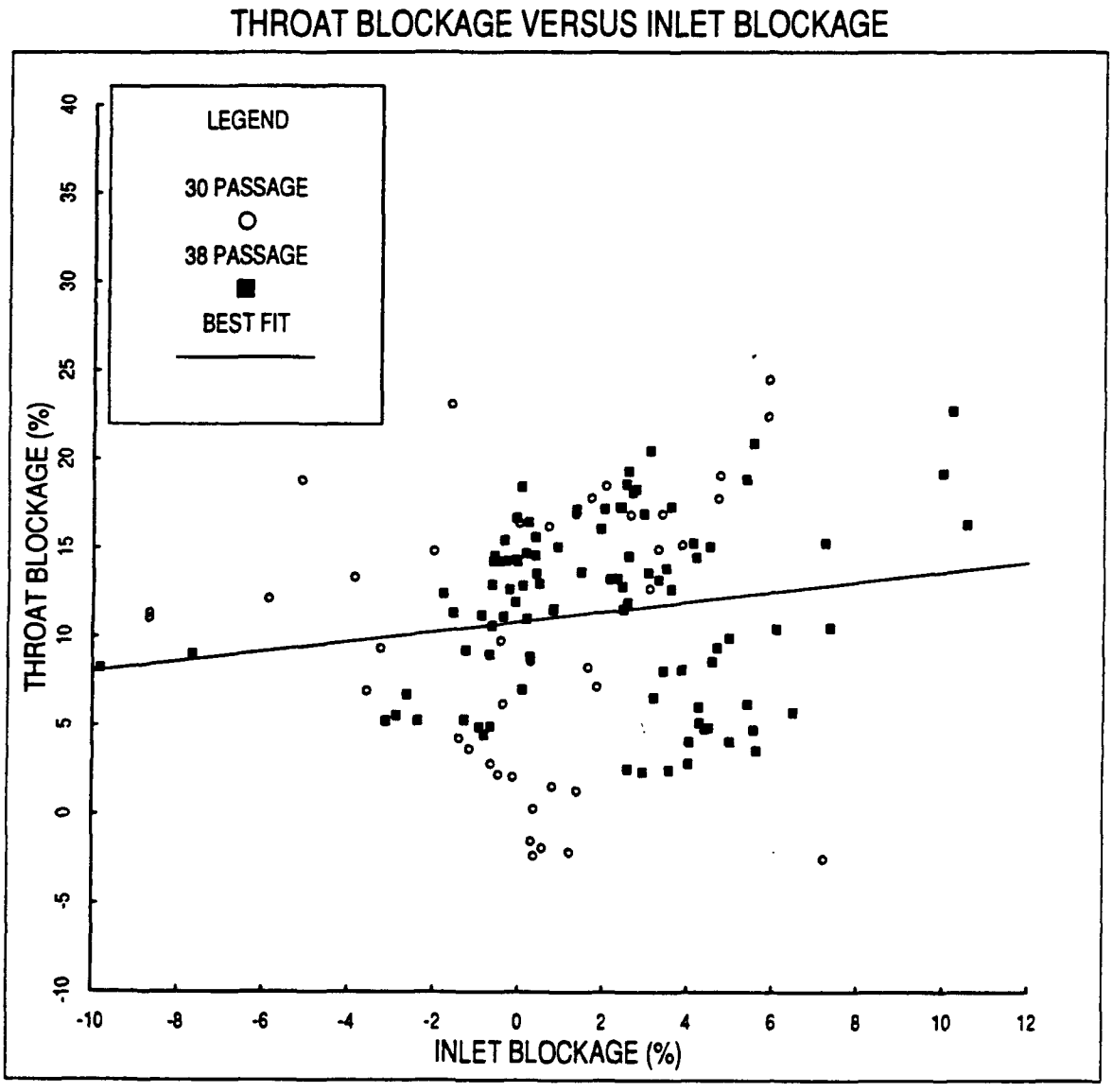


Figure 16: A comparison of the estimated throat blockage and the inlet blockage.

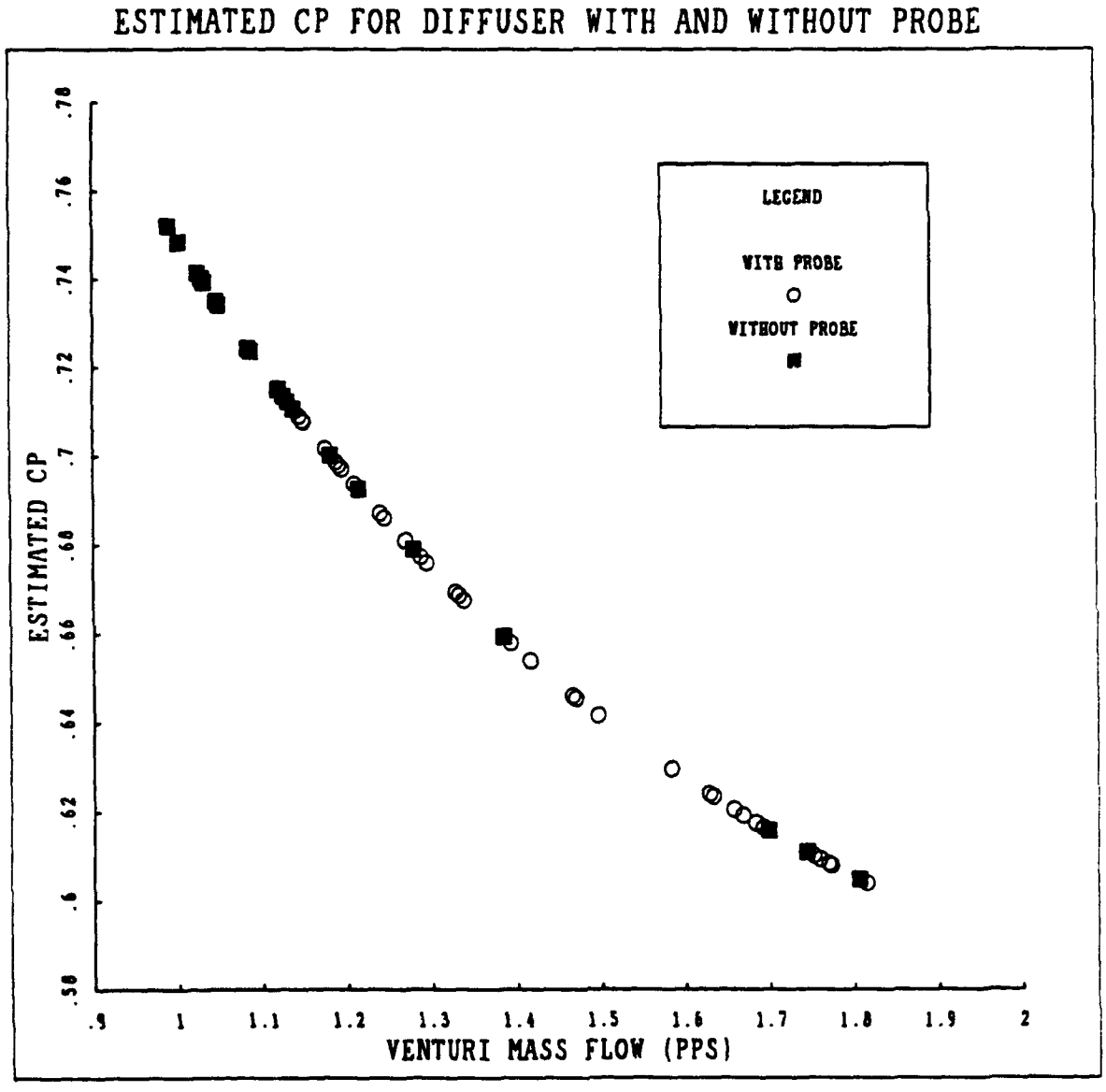


Figure 18: Estimated 4 KRPM speed line pressure rise coefficient for nominal inlet conditions, with and without traverse probe.

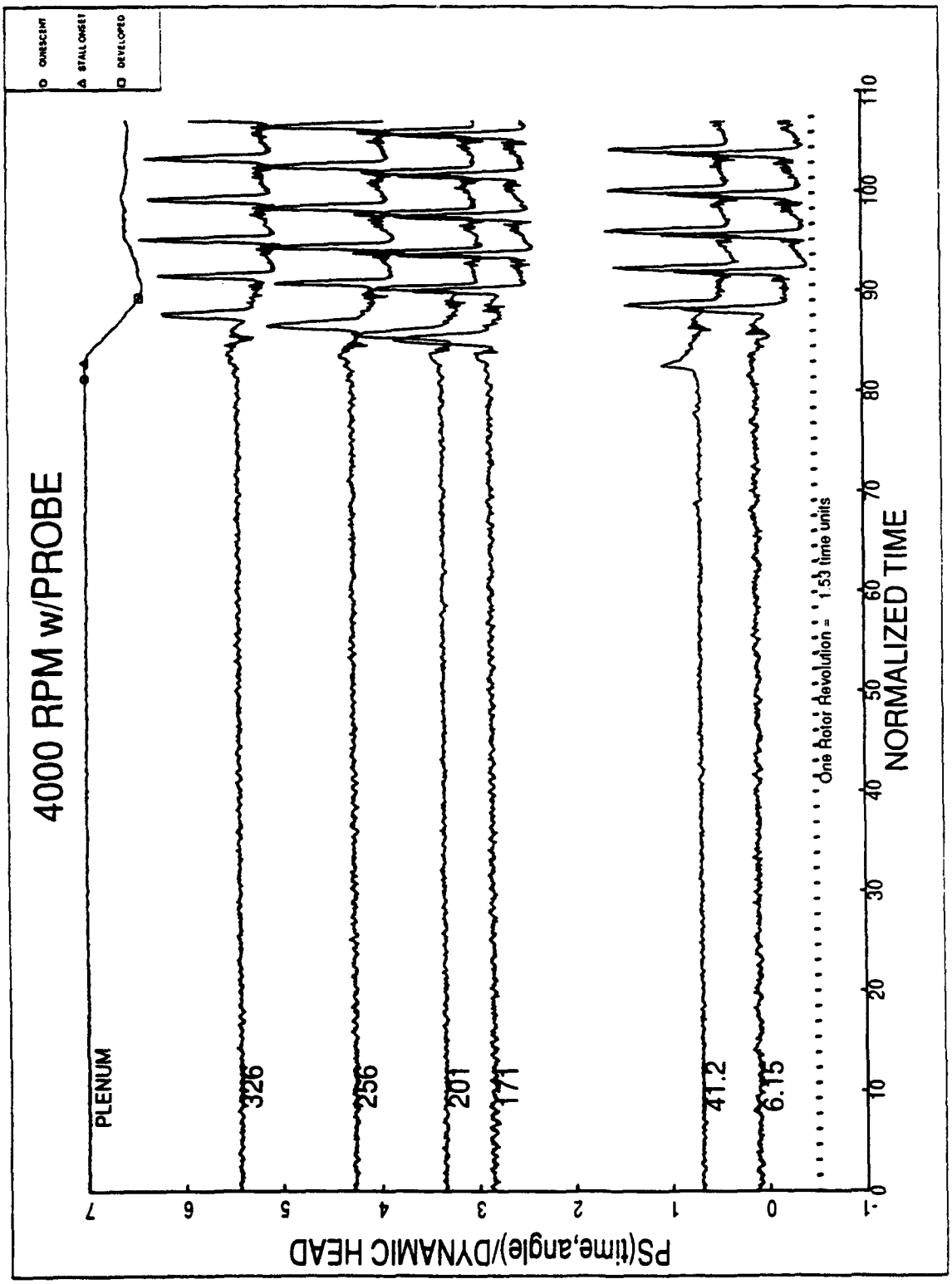


Figure 19: Nominal inlet, 4 KRPM high speed pressure data throttle to stall. Elapsed time was one second. Normalized time, $\tau$, is $t\sqrt{V_{\theta 1}}/2\pi r_1$.

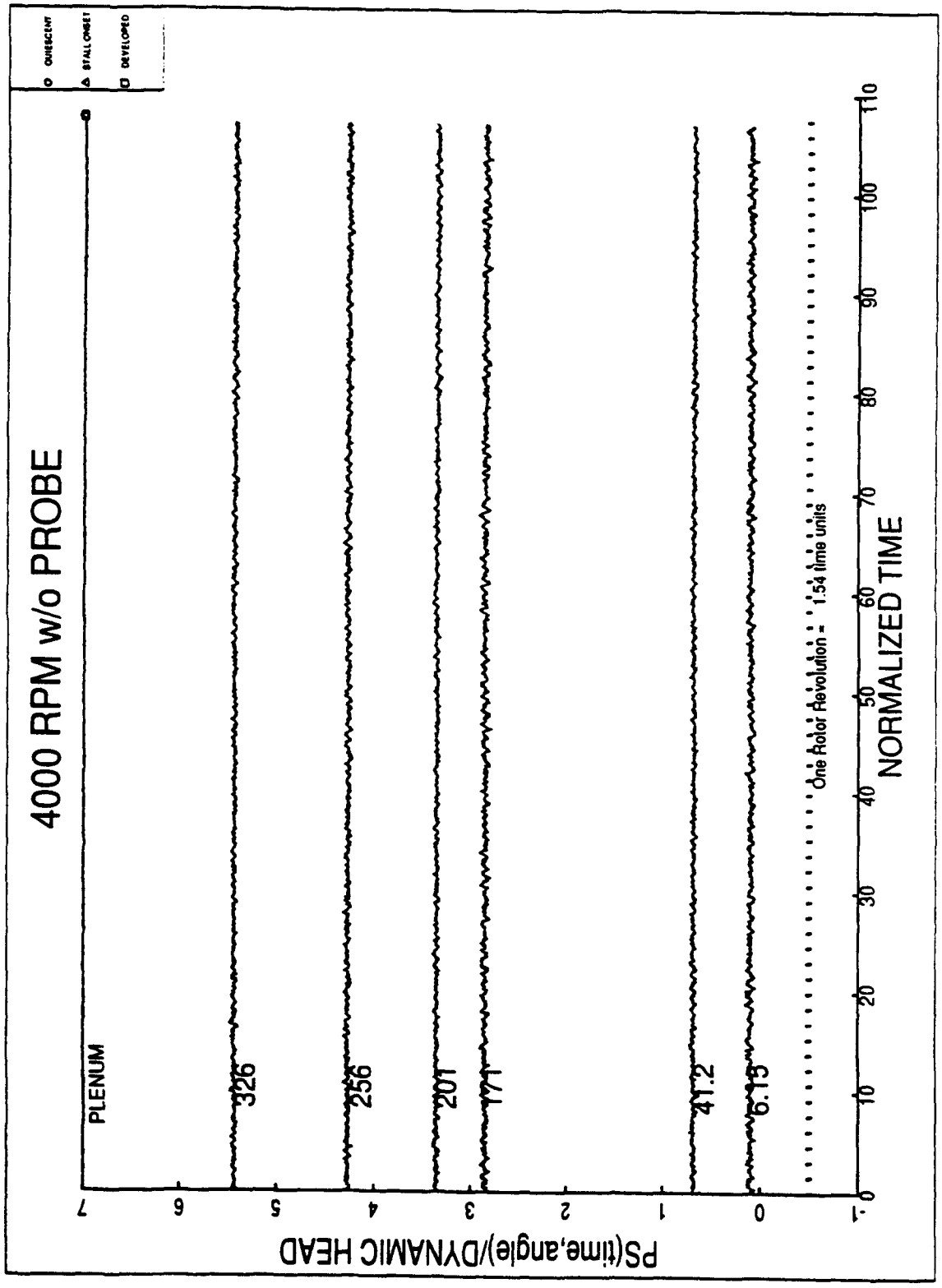


Figure 20: Nominal inlet, no traverse probe, 4 KRPM at the operating point at which the diffuser stalls when the probe is installed. Normalized time, $\tau$, is $t\overline{V_{\theta 1}}/2\pi r_1$.

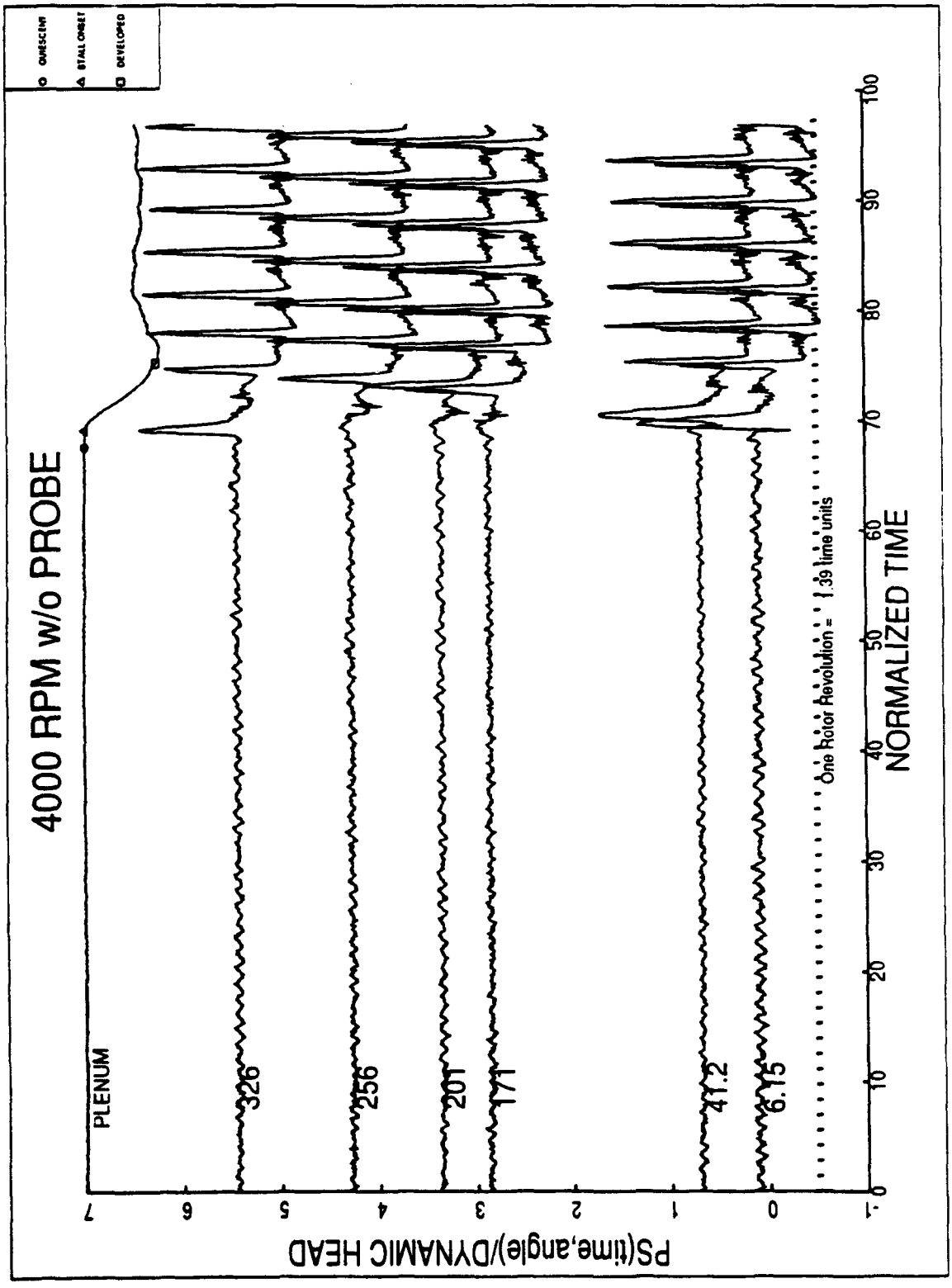


Figure 21: Nominal inlet, no traverse probe, 4 KRPM high speed pressure data throttle to stall. Elapsed time was one second. Normalized time, $\tau$, is $t\sqrt{V_{\theta 1}}/2\pi r_1$.